J. Fluid Mech. (2021), *vol*. 920, R3, doi:10.1017/jfm.2021.480

An exceptional point switches stability of a thermoacoustic experiment

Abdulla Ghani[1],† **and Wolfgang Polifke**[2]

[1]Department of Mechanical Engineering and Transport Systems, Technical University of Berlin, 10623 Berlin, Germany

[2]Department of Mechanical Engineering, Technical University of Munich, D-85748 Garching, Germany

(Received 22 February 2021; revised 23 April 2021; accepted 4 May 2021)

We identify an exceptional point in the numerical stability map of a combustion experiment operated with laminar premixed flames. A low-order model of the experiment allows one to investigate the interplay between the system modes and an exceptional point. The latter is located in the unstable region of the complex eigenvalue plane. Under gradual variation of the operating parameters, the branch-switching characteristic of the exceptional point can facilitate abrupt changes between strong instability and stable operation. The results also indicate that intrinsic thermoacoustic feedback plays an important role in the stability characteristics of this experiment.

Key words: low-dimensional models

1. Introduction

An unsteady flame, which manifests itself in heat release fluctuations $\dot{Q}'$, produces acoustic waves (Strahle 1971; Brear *et al.* 2012; Ghani & Poinsot 2017). In the case of an enclosed flame, the acoustic properties of the cavity and the flame dynamics define a phase lag between fluctuations of heat release $\dot{Q}'$ and pressure p'. For phase lags in the range $-\pi/2$ to $\pi/2$, the energy released by the flame is transferred to the acoustic field. For such cases, pressure waves grow in amplitude and attain sound levels up to 150 dB (Rayleigh 1878). This self-excited phenomenon is referred to as thermoacoustic instability (Candel 2002; Lieuwen & Yang 2005).

The description of the underlying feedback loop between acoustics, fluid dynamics and combustion is challenging and important since (i) fundamental research is required to avoid the occurrence of thermoacoustic instabilities and (ii) the resulting thermoacoustic instabilities can cause fatal damage to combustion applications, e.g. gas turbines,

† Email address for correspondence: ghani@tu-berlin.de

rocket engines and domestic boilers. This makes thermoacoustic instabilities a technical barrier to novel low-emission energy generation systems (Poinsot 2017).

Although intense research on thermoacoustic instabilities started in the 1950s, an important mechanism of instability was discovered only in 2014: theoretical, numerical and experimental studies indicate that a velocity-sensitive flame can trigger thermoacoustic instabilities even in perfectly anechoic acoustic conditions, hence, without any coupling with the acoustic eigenfrequencies of the combustor cavity. This instability mechanism is governed by the flame parameters (e.g. shape and length) rather than by the cavity acoustics: a pressure wave, generated by the unsteady flame, travels upstream and impinges upon the flame anchoring position to again provoke perturbations, which cause the unsteady flame to produce pressure waves. Consequently, this flame-intrinsic instability mechanism is termed as the intrinsic thermoacoustic (ITA) feedback loop (Hoeijmakers *et al.* 2014; Bomberg, Emmert & Polifke 2015; Courtine, Selle & Poinsot 2015; Emmert, Bomberg & Polifke 2015). Associated ITA modes were first reported for experiments in anechoic acoustic environments (Hoeijmakers *et al.* 2016) and later in situations where the acoustic boundaries are partially or fully reflective (Albayrak *et al.* 2018; Murugesan *et al.* 2018; Ghani *et al.* 2019). This renders ITA modes generally important in thermoacoustic studies.

Mathematically, combustion systems can be represented as dynamical systems: linear stability analysis yields the eigenfrequencies of the system and determines whether initial perturbations of infinitesimal amplitude grow or decay in time. These amplitudes may be associated with acoustic or ITA modes, as both appear in the complex plane. Acoustic systems with energy exchange, such as thermoacoustic systems, require a non-Hermitian description, which can feature exceptional points (EPs) where two (or more) modes coalesce in their eigenvalues and the corresponding eigenvectors (Latinne *et al.* 1995; Cartarius, Main & Wunner 2007; Doppler *et al.* 2016; Aurégan & Pagneux 2017; Goldzak, Mailybaev & Moiseyev 2018). EPs, also known as non-Hermitian degeneracies or branch points, have attracted wide attention across physics, e.g. applications are found in nanophotonics for light manipulation (Miri & Alu 2019), in single-mode lasers to decrease the fluctuating level of lasers (Feng *et al.* 2014) or in augmenting the quality of sensors (Wiersig 2020). One reason for these recent advances relies on the particular properties of EPs, as in their vicinity the parameter sensitivity becomes infinite and leads to a sudden state change of the system (Heiss 2012).

In thermoacoustics, EPs were described first by Mensah *et al.* (2018), who studied a theoretical configuration: by variation of two parameters of a simple flame model, acoustic and ITA modes coalesce in their eigenvalues and eigenfunctions in a specific point of parameter space. Close to an EP, the trajectories of both acoustic and ITA modes do not traverse the branch-point singularity, but feature strong veering and variation of the eigenvalues close to the EP even for small parameter changes. This is caused by the infinite sensitivity of EPs to parameter variations. Similar results were computed previously in thermoacoustic spectra without detailed explanations (Magri 2019; Silva, Yong & Magri 2019). Orchini *et al.* (2020) confirmed the mode veering feature of EPs in three-dimensional configurations, where longitudinal and azimuthal modes were considered. Recently, Schaefer, Guo & Polifke (2021) reported on an EP that was located in the stable complex plane.

Despite the richness of physical phenomena near EPs, their occurrence in combustion experiments has not been verified so far. In this paper, we provide evidence of an unstable EP in the stability map of a combustion experiment. This theoretical study highlights a key feature of EPs: the stability of the combustor is flipped from unstable to stable due to the typical branch-switching behaviour of EPs. Our analysis is based on linear acoustics

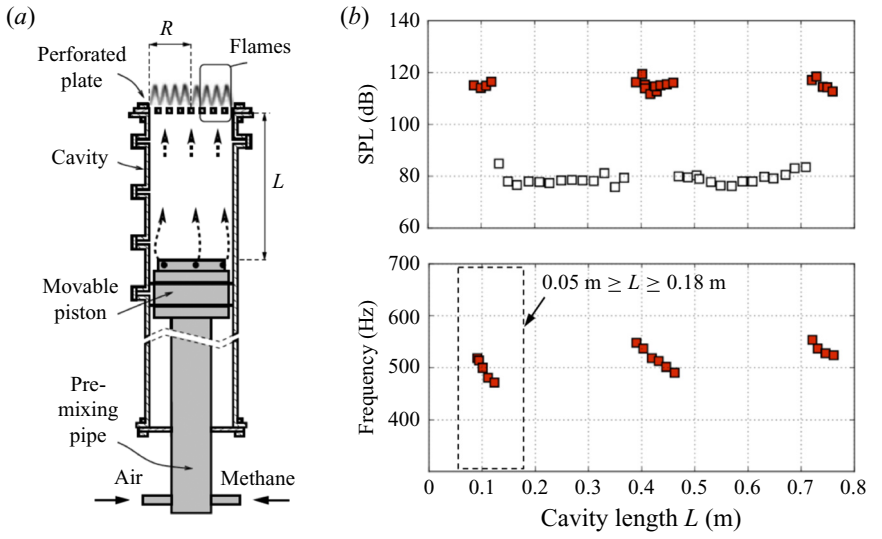

Figure 1. (*a*) Schematic view of the experimental set-up. (*b*) Instability frequencies and sound pressure level (SPL) reproduced from Noiray *et al.* (2007). Filled red markers denote unstable combustion. The frame displays the cavity lengths studied in this work.

combined with an empirical model for the flame. This well-established framework aims at (i) reproducing the experimental observations and (ii) exploring the impact of the EP on the system stability.

The paper is structured as follows. Next, § 2 describes the experimental set-up and summarizes the observations on combustor stability. Then, in § 3 we present the acoustic network model of the test rig supplemented with a decoupling strategy to identify the nature of unstable thermoacoustic modes. Finally, in § 4 we identify an EP in the numerical stability map by inspecting the transition process from unstable to stable combustion.

2. Experimental set-up and stability map

The experiment by Noiray *et al.* (2008) (figure 1*a*) consists of a cylindrical cavity ($R = 0.035$ m) with a movable piston, which allows one to modify the cavity length in the range $0.10\ \text{m} < L < 0.75\ \text{m}$. Air and methane are premixed at an equivalence ratio of $\phi = 0.86$ and enter the plenum with a mean velocity $u = 1.2\ \text{m s}^{-1}$ at ambient pressure ($\bar{p} = 1$ bar) and temperature ($\bar{T} = 300$ K). An ensemble of 420 laminar flames are stabilized at a perforated plate, where each hole has a radius of 1 mm. The plate thickness is 0.03 m. Pressure fluctuations are measured 0.35 m downstream of the flame location. These data provide the frequency of instability and the noise levels as functions of the length of the cavity (figure 1*b*): noise levels of 120 dB are measured for cavity lengths of 0.10 m, 0.40 m and 0.75 m (filled red markers). For other cavity lengths, distinct instability frequencies were not reported, but sound pressure levels remain at approximately 80 dB (Noiray 2007; Noiray *et al.* 2007). It is often observed that oscillation amplitudes grow gradually in response to changes in control parameters such as thermal power, equivalence ratio or plenum length. In the case considered here, changes in cavity length cause rather abrupt bifurcations in stability, which is a conspicuous point: noise levels switch abruptly between ∼80 dB and ∼120 dB (figure 1*b*).

A key parameter to formulate an acoustic flame element is the flame transfer function (FTF). It relates upstream velocity fluctuations u'_u to heat release fluctuations $\dot{Q}'$ that are

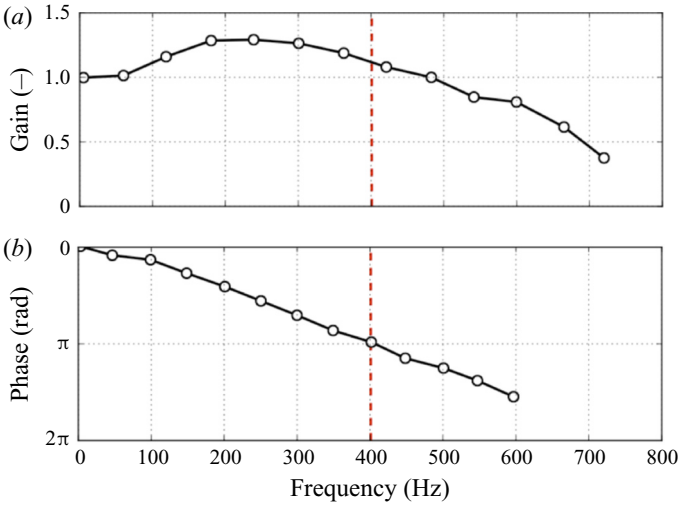

Figure 2. Experimentally measured FTF by Noiray *et al.* (2008) with $u'/\bar{u} = 0.34$. The red vertical dashed line indicates the frequency at which the $-\pi$ isoline is crossed.

normalized by their respective mean values (denoted by overbars):

$$F(\omega) = \frac{\dot{Q}'(\omega)/\bar{\dot{Q}}}{u'_u(\omega)/\bar{u}_u}, \quad \omega \in \mathbb{R}. \tag{2.1}$$

The FTF was measured by Noiray *et al.* (2008) and is plotted in figure 2. Note that the phase crosses the $-\pi$ isoline at 400 Hz. Previous studies identified that the phase of the FTF when crossing the $-\pi$ isoline predicts the frequency of the ITA mode in anechoic conditions (Hoeijmakers *et al.* 2014; Courtine *et al.* 2015; Emmert *et al.* 2015; Albayrak *et al.* 2018). We will discuss the relevance of this observation in § 4.

3. Model of the experiment

We model the combustion instabilities by linear acoustics combined with a model for the flame dynamics, which is a well-established framework for thermoacoustic studies (Keller 1995; Dowling 1997; Morgans & Dowling 2007; Juniper & Sujith 2018). The philosophy is a divide-and-conquer modelling approach: the entire experiment is divided into well-defined acoustic subsystems, for which analytical relations are written to describe the propagation of one-dimensional plane waves at the speed of sound. Each acoustic subsystem describes how the outgoing waves depend on the incoming waves. The ensemble of subsystems then describes the entire combustion system. We use a state-space formulation to (i) interconnect the individual subsystems to the complete system and (ii) facilitate the computation of the eigenvalues (Schuermans 2003; Emmert *et al.* 2016). Essential physical dynamics, i.e. frequency, growth rate and mode shape of every system mode, are computed within seconds on a standard workstation. Clearly, essential physical insight and low computational cost are major advantages of this approach compared to high-fidelity computational fluid dynamics approaches for reacting flows (Poinsot 2017).

The experimental model of interconnected acoustic subsystems contains two reflective ends, two ducts (cavity and channel inside the perforated plate), two area jumps (before and after the channel) and the flame element (figure 3). The flame is included as a compact element that obeys the linearized Rankine–Hugoniot jump conditions (Chu 1953).

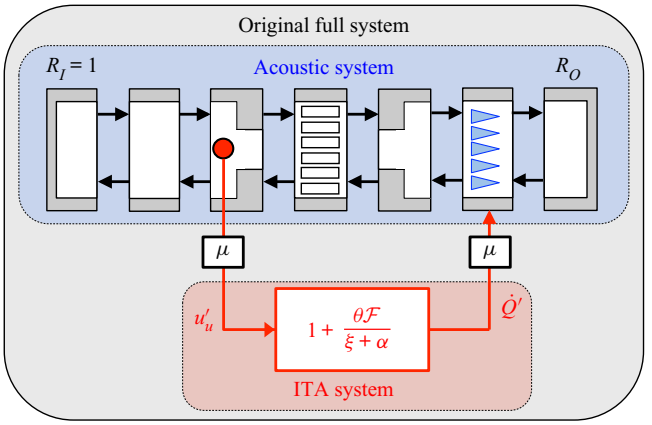

Figure 3. Representation of the full thermoacoustic system as an ITA system coupled to an acoustic system.

(The geometrical extension of the flames is approximately 0.01 m, whereas the unstable acoustic wavelengths $\lambda = c/f \approx 350\ \mathrm{m\ s^{-1}}/500\ \mathrm{Hz} \approx 0.7$ m are roughly 70 times larger.) To close the set of equations, a model for the flame dynamics, the FTF, is used (figure 2). Following Subramanian *et al.* (2015) and Albayrak *et al.* (2018), we use a rational function with optimized model parameters to fit accurately the measured FTF. The reflection coefficients for the piston, which represents the inlet of the model, and for the outlet are reported by Noiray (2007): while the inlet reflection coefficient is close to a hard wall ($R_I = 1$), the expression for the reflection coefficient at the outlet R_O given by Noiray (2007) contains the acoustic contributions of both the perforated plate and the flame. In the present study, we wish to clearly distinguish between the acoustic and ITA modes. It is then appropriate to employ separate acoustic elements, one for the flame dynamics and one for the reflection coefficient (figure 3). The present study employs the well-known model of Levine & Schwinger (1948) for the outlet reflection in simplified form (Munjal 1987):

$$R_O = (1 - \tfrac{1}{2}k^2R^2)\exp[\mathrm{i}(\pi - \tfrac{6}{5}\tan^{-1}(kR))], \tag{3.1}$$

where $k = \omega/c$ is the wavenumber with angular frequency $\omega = 2\pi f$ and speed of sound c. The amplitude and phase of (3.1) start at 1 and π, respectively, and decrease with increasing frequency. This model for an unflanged tube exit is widely employed in thermoacoustic studies (Moeck *et al.* 2009; Kraus, Selle & Poinsot 2018; Mukherjee 2018; Aguilar & Juniper 2020).

The dynamics of the state-space system is analysed by solving the linear eigenvalue problem:

$$(s\boldsymbol{I} - \boldsymbol{\mathcal{M}})\boldsymbol{x} = 0, \tag{3.2}$$

with the Laplace variable $s = \mathrm{i}\omega + \sigma$, the growth rate σ, the identity matrix $\boldsymbol{I}$ and the system matrix $\boldsymbol{\mathcal{M}}$. The eigenvalues are solved by computing the roots of the characteristic equation:

$$\det \boldsymbol{\mathcal{M}} = 0. \tag{3.3}$$

The system is linearly stable, i.e. initial perturbations are damped by the system if all eigenfrequencies have negative growth rates. Conversely, perturbations grow in time if one eigenfrequency has positive growth rate, which renders the system linearly unstable.

We compare the experimentally recorded limit-cycle frequencies against the model frequencies for linearly unstable modes parametrized by the cavity length L (figure 4).

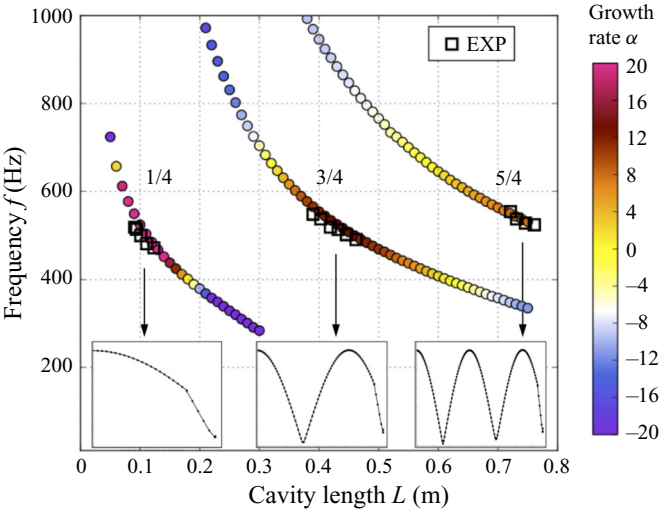

Figure 4. Validation of the model results against experimental limit-cycle frequencies reproduced from Noiray *et al.* (2007). The insets display the corresponding mode shapes in the cavity.

Overall, good agreement is found for the predicted frequencies, growth rates and stability limits. Note that frequencies and growth rates are subject to FTF as shown by Noiray *et al.* (2008). In this study, we only use the FTF measured with $u'/\bar{u} = 0.34$ (figure 2). The unstable modes correspond to the first, second and third quarter-wave modes of the cavity.

So far, the model of the experiment allows the thermoacoustic eigenvalues to be computed, but it does not allow an EP to be identified. To do so, we transform the system matrix $\boldsymbol{\mathcal{M}}$, without modifying its dynamics, to retrieve the following block structure:

$$0 = \underbrace{\left[\begin{array}{c|c} \boldsymbol{\mathcal{A}}_{sys} & \mu\boldsymbol{\mathcal{C}}_{F\to A} \\ \mu\boldsymbol{\mathcal{C}}_{A\to F} & \boldsymbol{\mathcal{F}}_{sys} \end{array}\right]}_{\boldsymbol{\mathcal{M}}} \underbrace{\left[\begin{array}{c} f_i \\ \vdots \\ g_x \\ u'_u \\ \dot{q}' \end{array}\right]}_{\boldsymbol{x}}. \tag{3.4}$$

The matrices $\boldsymbol{\mathcal{A}}_{sys}$ and $\boldsymbol{\mathcal{F}}_{sys}$ model the acoustic and the ITA subsystems, respectively. The cross-coupling of these two systems is described by the off-diagonal block matrices $\boldsymbol{\mathcal{C}}_{F\to A}$ and $\boldsymbol{\mathcal{C}}_{A\to F}$, where the indices indicate the impact of the flame on the acoustics and *vice versa*.

Now, the advantage of the block structure is that a coupling factor μ may be introduced, which decouples the original full system modes ($\mu = 1$) into an ITA system and an acoustic system ($\mu = 0$), as displayed in figure 3. The ITA system is described by $\boldsymbol{\mathcal{F}}_{sys}$. The acoustic system $\boldsymbol{\mathcal{A}}_{sys}$ provides the eigenfrequencies associated with the cavity modes while taking into account the temperature jump between the cold and hot gas regions ('passive flame'). A sweep from $\mu = 0 \to 1$ then identifies the nature of the full system mode. Setting $\mu = 0$, the dispersion relation reads

$$\det \boldsymbol{\mathcal{M}} = \underbrace{(Z_d\alpha - Z_u\xi)}_{\boldsymbol{\mathcal{A}}_{sys}} \underbrace{(\alpha + \xi + \theta\mathcal{F})}_{\boldsymbol{\mathcal{F}}_{sys}} = 0, \tag{3.5}$$

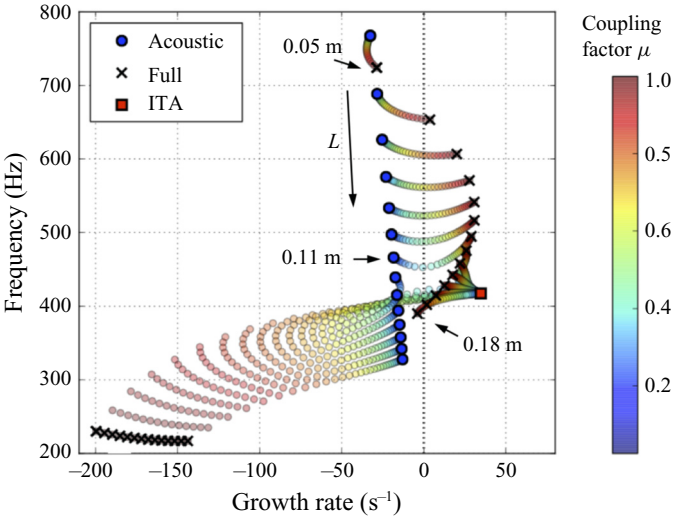

Figure 5. Eigenvalues computed for the full, ITA and acoustic systems (figure 3). The coupling factor traces the path of both acoustic and ITA systems ($\mu = 0$) to the original full system ($\mu = 1$). Cavity length is denoted as L, which varies from 0.05 m to 0.18 m. The acoustic and ITA modes are only computed for $\mu = 0$ at each cavity length. The acoustic mode for each cavity length corresponds to the first unstable mode.

where $\mathcal{F}$ is the complex-valued flame transfer function, $\theta = T_d/T_u - 1$ the specific ratio of temperatures up- and downstream of the flame, $\xi = (\rho_u c_u)/(\rho_d c_d)$ the ratio of specific acoustic impedances, α the area ratio of the plate cross-section and Z the acoustic impedance upstream (u) and downstream (d) of the flame. The factorized dispersion relation ((3.5)) separates the acoustic system $\boldsymbol{\mathcal{A}}_{sys}$ and the ITA system $\boldsymbol{\mathcal{F}}_{sys}$ eigenvalues.

This approach has been developed by Emmert *et al.* (2017) and associates (unstable) system modes with either acoustic or ITA modes. The procedure is briefly recapitulated in the Appendix. In this work, the coupling parameter is discretized into 40 increments to visualize the trajectories from both acoustic and ITA systems to the full system in a high-resolution parameter map.

4. Identification of exceptional points

With the model described above, which includes a decoupling feature, we report an EP in the numerical stability map of an experimental combustion device. To do so, two parameters are changed: (i) the cavity length L, which changes the acoustic modes, and (ii) the coupling parameter μ, which decouples the acoustic system from the flame dynamics, i.e. ITA system.

The stability map is shown in figure 5, where the abscissa displays the growth rate: the right half contains eigenfrequencies with positive growth rates, which yield unstable combustion. The computed eigenvalues correspond to cavity lengths $0.05\ \text{m} \leq L \leq 0.18\ \text{m}$, for which a switch from unstable to stable combustion is reported (figure 1*b*). Note that the smallest cavity length tested experimentally is 0.085 m. For the sake of brevity, we concentrate on this first transition from unstable to stable combustion. The same mechanism accounts for the stability transitions at $0.35\ \text{m} \leq L \leq 0.45\ \text{m}$ and $0.70\ \text{m} \leq L \leq 0.75\ \text{m}$ (figure 1*b*).

The ITA system is unstable at 418 Hz (figure 5, red square), which is coherent with the $-\pi$ criterion for the phase of the FTF (figure 2) (Hoeijmakers *et al.* 2014; Courtine

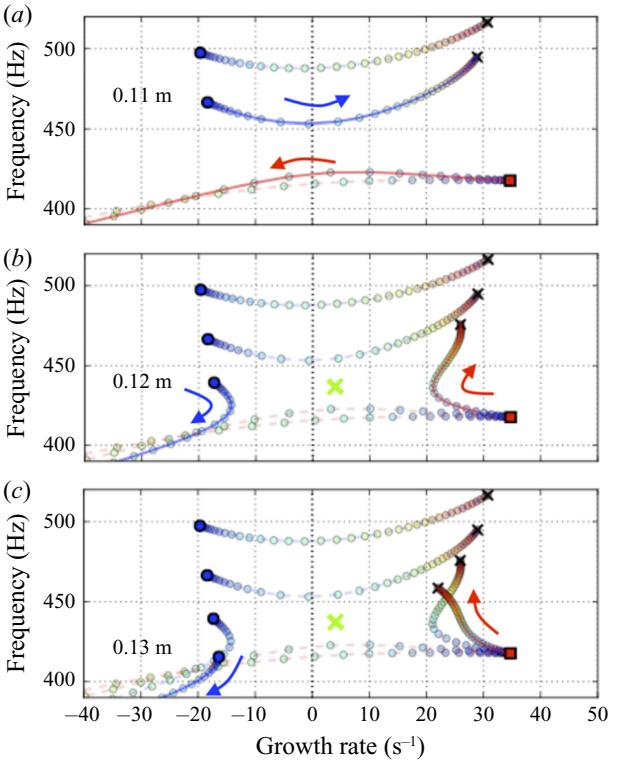

Figure 6. Branch switch and strong mode veering observed during change of cavity length L, featuring typical characteristics of an EP. The branch switch appears for $L = 0.12$ m in panel (b). Panels (a) and (c) display the nature of unstable modes before and after the branch switch, respectively. Arrows indicate increasing coupling factor. The expected EP location is marked with a cross.

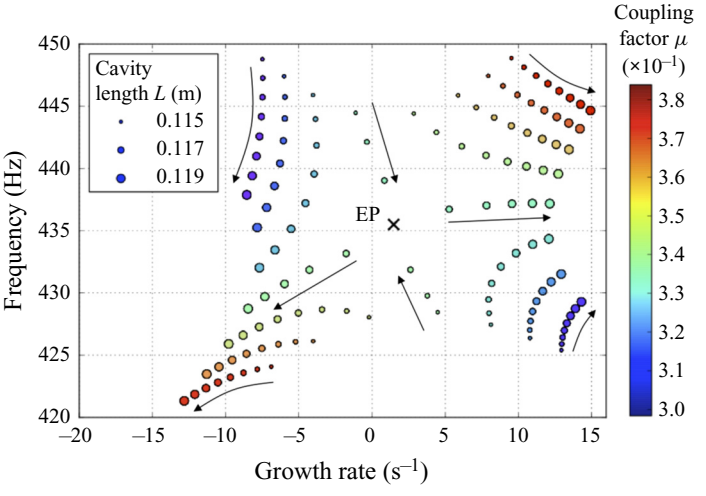

Figure 7. Computation of the exact EP location based on a contour integral method (Gavin *et al.* 2018). The cavity length L is varied from 0.115 m to 0.119 m (displayed by marker size) and the coupling factor μ from 0.30 to 0.38 (displayed by marker colour). The EP is located at $L = 0.168$ m and $\mu = 0.342$ (displayed by the cross marker).

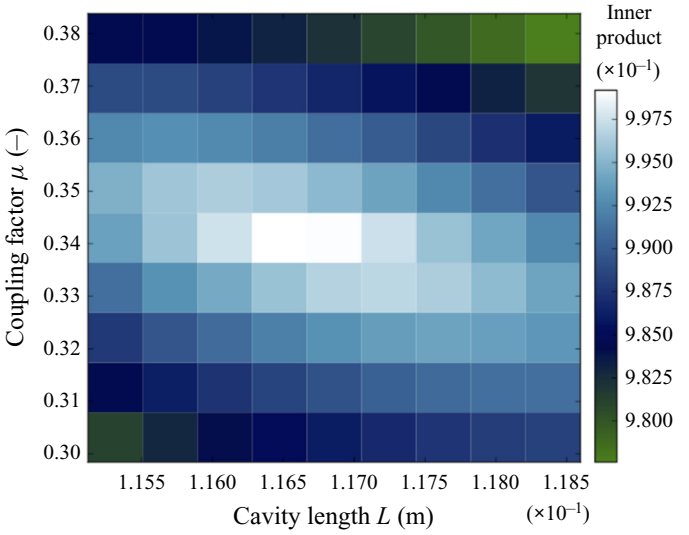

Figure 8. Inner product computation of the eigenvectors. Values close to unity indicate that the eigenvectors are parallel. The EP is located at $L = 0.168$ m and $\mu = 0.342$ (white panels).

et al. 2015; Emmert *et al.* 2015). For $L \leq 0.11$ m, the ITA mode couples to very strongly damped full system modes at approximately 210 Hz. In contrast, the acoustic modes couple to the unstable full system modes, for which the highest growth rates are found for frequencies around 510 Hz $\pm$ 5 Hz (figure 5), which is in agreement with experimental stability observations (figure 1*b*).

As the cavity length is further increased ($L \geq 0.12$ m), the nature of the unstable full system mode changes: now, the acoustic modes couple to the strongly damped full system modes at approximately 210 Hz, whereas the ITA mode couples to the unstable full system modes.

Figure 6 highlights the change in mode nature in more detail. Figure 6(*a*), for $L = 0.11$ m, shows that the acoustic modes couple to the unstable full system mode, while the ITA mode couples to damped modes at approximately 210 Hz for $\mu = 1$. Figure 6(*b*) displays the stability map for $L = 0.12$ m. Conversely to figure 6(*a*), the damped full system mode originates from the acoustic mode and the ITA mode drives the unstable combustion process at frequencies of approximately 470 Hz. This change in mode nature is due to a branch switch. This pattern continues for the next cavity length $L = 0.13$ m (figure 6*c*) but growth rates start to decay. Further increase of the cavity length $L > 0.13$ m drastically decreases the growth rates until the unstable mode becomes stable (figure 5). The location of the EP is roughly estimated as the intersection of the average mode distances in the area where no modes are active.

To confirm the location of the EP, we use a contour integral method (Gavin, Miedlar & Polizzi 2018) as done by Mensah *et al.* (2018). Next, we applied the method to the present target configuration (figure 7). By varying the cavity length L and the coupling parameter μ in a small range, we found the exact location of the EP to be close to the estimated location (figure 6). Figure 7 features another property of EPs: when varying the cavity length for the constant coupling parameter $\mu = 0.34$, the eigenvalue trajectories collide from opposite directions at the EP and, for further increase of L, veer off in a perpendicular direction. As discussed in Seyranian, Kirillov & Mailybaev (2005) and Mensah *et al.* (2018), this veering pattern is a unique feature of EPs. Finally, we show that the inner product of the

eigenfunction close to the EP is approximately unity (figure 8): this demonstrates that, at the EP, the eigenvalues and the corresponding eigenfunctions coalesce.

In this work, the most striking consequences of an EP are found: (i) a region indicating large parameter sensitivities, (ii) where strong veering of mode paths is found (figure 5), and (iii) a branch switch that changes the nature of the instability (figure 6). We confirmed our results by computing the exact EP location and the corresponding (almost perfectly) parallel eigenvectors for the same frequency. The branch-switching behaviour provides a possible explanation for the experimentally observed sudden change in noise levels between 80 dB and 120 dB (figure 1*b*). We also highlight the fact that the ITA mode plays a significant role in the stability of this set-up. To the best of our knowledge, this point has not been reported before.

5. Conclusion

Only recently, the theoretical studies of Mensah *et al.* (2018) featured EPs located in the stable complex plane of prototypical, canonical test cases. In this study, we identify an unstable EP in the numerical stability map of an experimental combustion system. By tracing the nature of the full system modes, the mode paths displayed strong veering and a branch switch close to the EP. The latter was found in the unstable complex plane and triggered stability transition. The results reveal that the ITA feedback loop plays an important role in this stability transition.

The identification of EPs requires two parameters to be changed. In this study, we propose a numerical tool to study EPs that uses one physical parameter (the cavity length L) together with a 'virtual parameter' (the coupling parameter μ, which decouples the full system into acoustic and ITA modes to understand the nature of the thermoacoustic mode): it can also be used to reduce the experimental complexity of the set-up, as only one variation is needed instead of two.

Future work will focus on the impact of nonlinear forcing amplitudes to incorporate the experimentally reported Flame Describing Function.

Acknowledgements. We thank the anonymous reviewers whose comments helped to improve this paper.

Declaration of interests. The authors report no conflict of interest.

Author ORCIDs.
Abdulla Ghani https://orcid.org/0000-0002-8029-1244;
Wolfgang Polifke https://orcid.org/0000-0001-7058-6498.

Appendix. Acoustic network model

Fluctuations of velocity u' and pressure p' are linked via characteristic wave amplitudes:

$$f = \frac{1}{2}\left(\frac{p'}{\rho c} + u'\right), \quad g = \frac{1}{2}\left(\frac{p'}{\rho c} - u'\right). \tag{A1a,b}$$

From (A1), primitive variables can be computed via $u' = f - g$ and $p'/\rho c = f + g$. The ratio of the characteristic waves describes reflection coefficients as $R_u = g_u/f_u$ and $R_d = f_d/g_d$. Using the definition of the acoustic impedance, these can be written as

$$\left.\begin{aligned} R_u &= (Z_u + 1)/(Z_u - 1), \\ R_d &= (Z_d - 1)/(Z_d + 1). \end{aligned}\right\} \tag{A2}$$

The configuration shown in figure 3 contains acoustic elements up- and downstream of the flame, which can be lumped together as impedances Z_u and Z_d, respectively. Considering the flame as a compact element, the Rankine–Hugoniot jump conditions (Chu 1953) formulate an acoustic flame model. Combining the compact flame element together with the upstream cross-sectional area change (figure 3), the scattering matrix is

$$\begin{bmatrix} f_u \\ g_d \end{bmatrix} = \begin{bmatrix} \dfrac{\alpha-\xi}{\alpha+\xi} & \dfrac{2}{\alpha+\xi} & \dfrac{\theta}{\alpha+\xi} \\ \dfrac{2\alpha\xi}{\alpha+\xi} & \dfrac{\xi-\alpha}{\alpha+\xi} & \dfrac{\xi\theta}{\alpha+\xi} \end{bmatrix} \begin{bmatrix} f_d \\ g_u \\ \dot{q}' \end{bmatrix}, \tag{A3}$$

where $\dot{q}' = F(\omega)u_u'$ with $u_u' = f_u - g_u$. The system matrix $\mathcal{M}$ is obtained by combining (A2) and (A3):

$$0 = \underbrace{\begin{bmatrix} -1 & \dfrac{Z_u+1}{Z_u-1} & 0 & 0 & 0 & 0 \\ \dfrac{\alpha-\xi}{\alpha+\xi} & -1 & 0 & \dfrac{2}{\alpha+\xi} & 0 & \dfrac{\theta}{\alpha+\xi} \\ \dfrac{2\alpha\xi}{\alpha+\xi} & 0 & -1 & \dfrac{\xi-\alpha}{\alpha+\xi} & 0 & \dfrac{\xi\theta}{\alpha+\xi} \\ 0 & 0 & \dfrac{Z_d-1}{Z_d+1} & -1 & 0 & 0 \\ 1 & -1 & 0 & 0 & -1 & 0 \\ 0 & 0 & 0 & 0 & F & -1 \end{bmatrix}}_{\mathcal{M}} \begin{bmatrix} f_u \\ g_u \\ f_d \\ g_u \\ u_u' \\ \dot{q}' \end{bmatrix}, \tag{A4}$$

Emmert *et al.* (2017) proposed to separate out the upstream outgoing wave g_u caused by the flame. From (A4), we find that (i) the heat release $\dot{q}'$ drives g_u via $\theta/(\alpha+\xi)$, (ii) g_u acts on $(Z_u+1)/(Z_u-1)$ via the upstream ingoing wave f_u and (iii) g_u also acts on the velocity fluctuation u_u' by -1. The equations are rearranged such that $\dot{q}'$ directly affects f_u and the coupling term μ is introduced:

$$0 = \underbrace{\left[\begin{array}{cccc|cc} -1 & \dfrac{Z_u+1}{Z_u-1} & 0 & 0 & 0 & \mu\dfrac{Z_u+1}{Z_u-1}\dfrac{\theta}{\alpha+\xi} \\ \dfrac{\alpha-\xi}{\alpha+\xi} & -1 & 0 & \dfrac{2}{\alpha+\xi} & 0 & 0 \\ \dfrac{2\alpha\xi}{\alpha+\xi} & 0 & -1 & \dfrac{\xi-\alpha}{\alpha+\xi} & 0 & \mu\dfrac{\xi\theta}{\alpha+\xi} \\ 0 & 0 & \dfrac{Z_d-1}{Z_d+1} & -1 & 0 & 0 \\ \hline \mu & -\mu & 0 & 0 & -1 & -\dfrac{\theta}{\alpha+\xi} \\ 0 & 0 & 0 & 0 & F & -1 \end{array}\right]}_{\mathcal{M}} \begin{bmatrix} f_u \\ g_u \\ f_d \\ g_u \\ u_u' \\ \dot{q}' \end{bmatrix}. \tag{A5}$$

By transforming the system, the dynamics are not modified, thus the characteristic equation and eigenvalues do not change, but now the system has a block matrix structure (3.4).

References

Aguilar, J.G & Juniper, M.P. 2020 Thermoacoustic stabilization of a longitudinal combustor using adjoint methods. *Phys. Rev. Fluids* **5** (8), 083902.

Albayrak, A., Steinbacher, T., Komarek, T. & Polifke, W. 2018 Convective scaling of intrinsic thermo-acoustic eigenfrequencies of a premixed swirl combustor. *Trans. ASME: J. Engng Gas Turbines Power* **140** (4), 41–51.

Aurégan, Y. & Pagneux, V. 2017 PT-symmetric scattering in flow duct acoustics. *Phys. Rev. Lett.* **118** (17), 174301.

Bomberg, S., Emmert, T. & Polifke, W. 2015 Thermal versus acoustic response of velocity sensitive premixed flames. *Proc. Combust. Inst.* **35** (3), 3185–3192.

Brear, M.J., Nicoud, F., Talei, M., Giauque, A. & Hawkes, E.R. 2012 Disturbance energy transport and sound production in gaseous combustion. *J. Fluid Mech.* **707**, 53–73.

Candel, S. 2002 Combustion dynamics and control: progress and challenges. *Proc. Combust. Inst.* **29** (1), 1–28.

Cartarius, H., Main, J. & Wunner, G. 2007 Exceptional points in atomic spectra. *Phys. Rev. Lett.* **99** (17), 173003.

Chu, B.-T. 1953 On the generation of pressure waves at a plane flame front. *Symp. (Intl) Combust.* **4** (1), 603–612.

Courtine, E., Selle, L. & Poinsot, T. 2015 DNS of intrinsic thermoacoustic modes in laminar premixed flames. *Combust. Flame* **162** (11), 4331–4341.

Doppler, J., Mailybaev, A.A., Böhm, J., Kuhl, U., Girschik, A., Libisch, F., Milburn, T.J., Rabl, P., Moiseyev, N. & Rotter, S. 2016 Dynamically encircling an exceptional point for asymmetric mode switching. *Nature* **537** (7618), 76.

Dowling, A.P. 1997 Nonlinear self-excited oscillations of a ducted flame. *J. Fluid Mech.* **346**, 271–290.

Emmert, T., Bomberg, S., Jaensch, S. & Polifke, W. 2017 Acoustic and intrinsic thermoacoustic modes of a premixed combustor. *Proc. Combust. Inst.* **36** (3), 3835–3842.

Emmert, T., Bomberg, S. & Polifke, W. 2015 Intrinsic thermoacoustic instability of premixed flames. *Combust. Flame* **162** (1), 75–85.

Emmert, T., Meindl, M., Jaensch, S. & Polifke, W. 2016 Linear state space interconnect modeling of acoustic systems. *Acta Acust. United Acust.* **102** (5), 824–833.

Feng, L., Wong, Z.J., Ma, R.-M., Wang, Y. & Zhang, X. 2014 Single-mode laser by parity-time symmetry breaking. *Science* **346** (6212), 972–975.

Gavin, B., Miedlar, A. & Polizzi, E. 2018 Feast eigensolver for nonlinear eigenvalue problems. *J. Comput. Sci.* **27**, 107–117.

Ghani, A. & Poinsot, T. 2017 Flame quenching at walls: A source of sound generation. *Flow Turbul. Combust.* **99** (1), 173–184.

Ghani, A., Steinbacher, T., Albayrak, A. & Polifke, W. 2019 Intrinsic thermoacoustic feedback loop in turbulent spray flames. *Combust. Flame* **205**, 22–32.

Goldzak, T., Mailybaev, A.A. & Moiseyev, N. 2018 Light stops at exceptional points. *Phys. Rev. Lett.* **120** (1), 013901.

Heiss, W.D. 2012 The physics of exceptional points. *J. Phys.* A **45** (44), 444016.

Hoeijmakers, M., Kornilov, V., Arteaga, I.L., de Goey, P. & Nijmeijer, H. 2014 Intrinsic instability of flame–acoustic coupling. *Combust. Flame* **161** (11), 2860–2867.

Hoeijmakers, M., Kornilov, V., Arteaga, I.L., de Goey, P. & Nijmeijer, H. 2016 Flame dominated thermoacoustic instabilities in a system with high acoustic losses. *Combust. Flame* **169**, 209–215.

Juniper, M.P. & Sujith, R.I. 2018 Sensitivity and nonlinearity of thermoacoustic oscillations. *Annu. Rev. Fluid Mech.* **50**, 661–689.

Keller, J.J. 1995 Thermoacoustic oscillations in combustion chambers of gas turbines. *AIAA J.* **33** (12), 2280–2287.

Kraus, C., Selle, L. & Poinsot, T. 2018 Coupling heat transfer and large eddy simulation for combustion instability prediction in a swirl burner. *Combust. Flame* **191**, 239–251.

Latinne, O., Kylstra, N.J., Dörr, M., Purvis, J., Terao-Dunseath, M., Joachain, C.J., Burke, P.G. & Noble, C.J. 1995 Laser-induced degeneracies involving autoionizing states in complex atoms. *Phys. Rev. Lett.* **74** (1), 46.

Levine, H. & Schwinger, J. 1948 On the radiation of sound from an unflanged circular pipe. *Phys. Rev.* **73** (4), 383.

Lieuwen, T. & Yang, V. 2005 *Combustion instabilities in gas turbine engines. operational experience, fundamental mechanisms and modeling*. Progress in Astronautics and Aeronautics, vol. 210. AIAA.

Magri, L. 2019 Adjoint methods as design tools in thermoacoustics. *Appl. Mech. Rev.* **71** (2), 020801.

MENSAH, G.A., MAGRI, L., SILVA, C.F., BUSCHMANN, P.E. & MOECK, J.P. 2018 Exceptional points in the thermoacoustic spectrum. *J. Sound Vib.* **433**, 124–128.

MIRI, M.-A. & ALU, A. 2019 Exceptional points in optics and photonics. *Science* **363** (6422), eaar7709.

MOECK, J.P., OEVERMANN, M., KLEIN, R., PASCHEREIT, C. & SCHMIDT, H. 2009 A two-way coupling for modeling thermoacoustic instabilities in a flat flame Rijke tube. *Proc. Combust. Inst.* **32**, 1199–1207.

MORGANS, A.S. & DOWLING, A.P. 2007 Model-based control of combustion instabilities. *J. Sound Vib.* **299** (1–2), 261–282.

MUKHERJEE, N.K. 2018 Analytic description of flame intrinsic instability in one-dimensional model of open–open combustors with ideal and non-ideal end boundaries. *Intl J. Spray Combust.* **10** (4), 287–314.

MUNJAL, M.L. 1987 *Acoustics of ducts and mufflers with application to exhaust and ventilation system design*. John Wiley & Sons.

MURUGESAN, M., SINGARAVELU, B., KUSHWAHA, A.K. & MARIAPPAN, S. 2018 Onset of flame-intrinsic thermoacoustic instabilities in partially premixed turbulent combustors. *Intl J. Spray Combust. Dyn.* **10** (3), 171–184.

NOIRAY, N. 2007 Analyse linéaire et non-linéaire des instabilités de combustion: application aux systèmes à injection multipoints et stratégies de contrôle. PhD thesis, Laboratoire d'énergétique moléculaire et macroscopique, combustion (Gif-sur-Yvette, Essonne).

NOIRAY, N., DUROX, D., SCHULLER, T. & CANDEL, S. 2007 Passive control of combustion instabilities involving premixed flames anchored on perforated plates. *Proc. Combust. Inst.* **31**, 1283–1290.

NOIRAY, N., DUROX, D., SCHULLER, T. & CANDEL, S. 2008 A unified framework for nonlinear combustion instability analysis based on the flame describing function. *J. Fluid Mech.* **615**, 139–167.

ORCHINI, A., SILVA, C.F., MENSAH, G.A. & MOECK, J.P. 2020 Thermoacoustic modes of intrinsic and acoustic origin and their interplay with exceptional points. *Combust. Flame* **211**, 83–95.

POINSOT, T. 2017 Prediction and control of combustion instabilities in real engines. *Proc. Combust. Inst.* **36** (1), 1–28.

RAYLEIGH, LORD 1878 The explanation of certain acoustic phenomena. *Nature* **18**, 319–321.

SCHAEFER, F., GUO, S. & POLIFKE, W. 2021 The impact of exceptional points on the reliability of thermoacoustic stability analysis. *Trans. ASME: J. Engng Gas Turbines Power* **143** (2), 021010.

SCHUERMANS, B. 2003 Modeling and control of thermoacoustic instabilities. PhD thesis, Ecole Polytechnique Federale de Lausanne.

SEYRANIAN, A.P., KIRILLOV, O.N. & MAILYBAEV, A.A. 2005 Coupling of eigenvalues of complex matrices at diabolic and exceptional points. *J. Phys.* A **38** (8), 1723.

SILVA, C., YONG, K.J. & MAGRI, L. 2019 Thermoacoustic modes of quasi-one-dimensional combustors in the region of marginal stability. *Trans. ASME: J. Engng Gas Turbines Power* **141** (2), 021022.

STRAHLE, W.C. 1971 On combustion generated noise. *J. Fluid Mech.* **49**, 399–414.

SUBRAMANIAN, P., BLUMENTHAL, R.S., POLIFKE, W. & SUJITH, R.I. 2015 Distributed time lag response functions for the modelling of combustion dynamics. *Combust. Theor. Model.* **19** (2), 223–237.

WIERSIG, J. 2020 Review of exceptional point-based sensors. *Photon. Res.* **8** (9), 1457–1467.